CHEMISTRY OF MATERIALS

Article

pubs.acs.org/cm

Computational Prediction and Evaluation of Solid-State Sodium Superionic Conductors $Na_7P_3X_{11}$ (X = O, S, Se)

Yan Wang,*[,†,‡] William D. Richards,[†] Shou-Hang Bo,[§,#] Lincoln J. Miara,[‡] and Gerbrand Ceder*[,†,§,∥]

[†]Department of Materials Science and Engineering, Massachusetts Institute of Technology, Cambridge, Massachusetts 02139, United States

[‡]Advanced Materials Lab, Samsung Research America, 3 Van de Graaff Drive, Burlington, Massachusetts 01803, United States

[§]Materials Science Division, Lawrence Berkeley National Laboratory, Berkeley, California 94720, United States

[∥]Department of Materials Science and Engineering, University of California, Berkeley, California 94720, United States

ABSTRACT: Inorganic solid-state ionic conductors with high ionic conductivity are of great interest for their application in safe and high-energy-density solid-state batteries. Our previous study reveals that the crystal structure of the ionic conductor $Li_7P_3S_{11}$ contains a body-centered-cubic (bcc) arrangement of sulfur anions and that such a bcc anion framework facilitates high ionic conductivity. Here, we apply a set of first-principles calculations techniques to investigate $A_7P_3X_{11}$-type (A = Li, Na; X = O, S, Se) lithium and sodium superionic conductors derived from $Li_7P_3S_{11}$, focusing on their structural, dynamic and thermodynamic properties. We find that the ionic conductivity of $Na_7P_3S_{11}$ and $Na_7P_3Se_{11}$ is over 10 mS cm^{-1} at room temperature, significantly higher than that of any known solid Na-ion sulfide or selenide conductor. However, thermodynamic calculations suggest that the isostructural sodium compounds may not be trivial to synthesize, which clarifies the puzzle concerning the experimental problems in trying to synthesize these compounds.

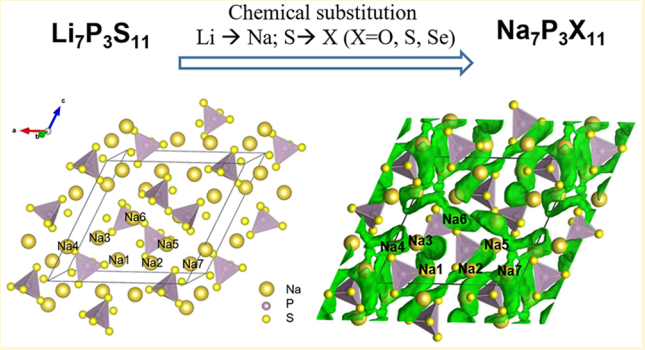

INTRODUCTION

Solid-state batteries that utilize a solid-state ionic conductor rather than a liquid electrolyte have great potential to provide safe and more energy dense batteries than today's Li-ion and Na-ion batteries.[1] The development of novel solid-state alkali ionic conductors has proceeded rapidly. The search for new inorganic ionic conductors is largely motivated by the need for high-ionic conductivities at room temperature (RT). A few recently discovered Li solid-state ionic conductors (e.g., $Li_{10}GeP_2S_{12}$ and $Li_7P_3S_{11}$) have superhigh ionic conductivities of over 10 mS cm^{-1} at RT, rivalling the performance of widely used organic liquid electrolytes.[2,3] The discovery of Na ionic conductors predates the high-conductivity materials used for Li (e.g., β- and β''-aluminas and NASICON),[4,5] but so far the use of Na ionic conductors has been limited due to the high-temperature sintering requirement, the relatively low ionic conductivity, or the limited electrochemical stability window. Multiple Na sulfides and selenides[6−10] (e.g., Na_3PS_4, Na_3PSe_4, Na_3SbS_4, and $Na_{10}SnP_2S_{12}$) have recently been found to have high ionic conductivities of over 0.1 mS cm^{-1}. These sulfides and selenides can also form dense pellets without high-temperature sintering, rendering a great advantage in materials processing. However, the Na-ion conductivities of these conductors are still quite limited and significantly lower than that of the liquid electrolytes, limiting their use in practical solid-state batteries.

Computational studies have played an important role in recent research of solid-state ionic conductors by providing insight into fundamental mechanisms that are not otherwise accessible and by predicting new ionic conductors with superior properties. First-principles computational techniques, such as density functional theory (DFT) calculations and ab initio molecular dynamics (AIMD) simulations, have proven to be quite accurate for predicting materials properties of high-performance lithium and sodium ionic conductors such as phase stability,[10,11] chemical and electrochemical stability,[12,13] hydrolysis stability,[14,15] mechanical properties,[16] and activation energy and ionic conductivity.[17−20] This predictive capability allows new materials to be screened before experimental synthesis. Examples include the computational prediction[10,11] and follow-up experimental confirmations of $Li_{10}SnP_2S_{12}$ (see ref 21), $Li_{10}SiP_2S_{12}$ (see refs 22 and23), and $Na_{10}SnP_2S_{12}$ (see ref 10) as affordable alternatives of the superionic conductor $Li_{10}GeP_2S_{12}$.

By investigation into the structural factors responsible for high Li-ion conductivity, we recently demonstrated that an underlying body-centered-cubic (bcc)-like anion framework, which allows direct Li migration between adjacent tetrahedral

Received: June 14, 2017
Revised: July 26, 2017
Published: July 27, 2017

DOI: 10.1021/acs.chemmater.7b02476
Chem. Mater. 2017, 29, 7475−7482

Table 1. Crystal Structural Parameters for DFT Calculated $Li_7P_3X_{11}$ and $Na_7P_3X_{11}$ (X = O, S, and Se)[a]

	lattice parameters						
	a (Å)	b (Å)	c (Å)	α (deg)	β (deg)	γ (deg)	unit-cell vol (Å^3)
$Li_7P_3O_{11}$	9.81	5.02	10.01	102.93	111.14	73.51	437.27
$Li_7P_3S_{11}$	12.84 (12.50)	6.21 (6.03)	12.65 (12.53)	103.87 (102.85)	113.84 (113.30)	73.90 (74.47)	876.18 (829.35)
$Li_7P_3Se_{11}$	13.55	6.49	13.38	103.58	113.45	74.19	1027.61
$Na_7P_3O_{11}$	10.94	5.58	10.86	103.25	114.12	71.23	568.93
$Na_7P_3S_{11}$	14.01	6.54	13.56	103.29	115.18	76.58	1080.62
$Na_7P_3Se_{11}$	15.12	6.85	13.96	103.97	115.60	76.74	1252.08

[a]The experimental reported values for $Li_7P_3S_{11}$ are included in parentheses.[36].

sites, is desirable for achieving high ionic conductivity.[24] Indeed, this anion arrangement is present in quite a few known superionic Li-conducting materials including the $Li_{10}MP_2S_{12}$ family (M = Ge, Si, and Sn) and $Li_7P_3S_{11}$. The bcc structural descriptor was also found to be applicable for Na-ion systems,[24] motivating our search for new Na ionic conductors with a bcc-type anion framework.

In this work, we apply well-developed first-principles computational techniques to search for new Na ionic conducting materials based on the bcc-type superionic conductor $Li_7P_3S_{11}$. Of all the considered chemical substitutions on the $Li_7P_3S_{11}$ framework to form $A_7P_3X_{11}$ (A = Li, Na; X = O, S, Se), molecular dynamics simulations predict large Na ionic conductivities of over 10 mS cm^{-1} in the Na substituted compounds $Na_7P_3S_{11}$ and $Na_7P_3Se_{11}$ at RT. Our DFT calculations clarify the competing roles of the anion and immobile cation host frameworks with regard to alkali ion migration. A detailed analysis of the Na energy landscape in the predicted compounds explains why the oxide version, $Na_7P_3O_{11}$, is predicted to have lower conductivity than $Na_7P_3S_{11}$ and $Na_7P_3Se_{11}$. Moreover, we investigate the thermodynamic stability of these ionic conductors through a detailed analysis of the computational phase diagrams including finite-temperature effects by phonon free energy calculations and suggest possible routes to synthesize the predicted sodium conductors.

METHODS

DFT Structural Optimization and Total-Energy Calculations. First-principles calculations were performed using density functional theory as implemented in the plane-wave-basis-set Vienna ab initio simulation package[25] (VASP). Projector augmented wave potentials with kinetic energy cutoff of 520 eV were employed in all structural optimizations and total-energy calculations, and the exchange and correlation functionals were described within Perdew–Burke–Ernzerhof generalized gradient approximation (GGA-PBE).[26] A k-point density of at least 500 per number of atoms in the unit cell was used in all calculations.

Crystal Structure Framework Matching. A structural matching algorithm implemented in the python materials genomics (pymatgen) package[27] was used to evaluate how well the anion sublattice of a compound maps onto a bcc framework, as in our previous study[24] for ionic conductors $Li_{10}GeP_2S_{12}$ and $Li_7P_3S_{11}$. The algorithm finds possible affine mappings which can transform the anion lattice exactly onto lattice points belonging to the perfect bcc lattice and chooses the mapping with the minimal root-mean-square (rms) distance between the atom positions in the two lattices. Only affine transformations preserving the bcc supercell lattice angles to within 5° and supercell lattice vector lengths to within 20% are considered, and the maximum allowed rms distance is set to be $0.4(V/n)^{1/3}$, where V/n is the normalized volume by number of atoms. The structural matching results are visualized using VESTA.[28]

Na-Ion Diffusivity and Conductivity Calculations. The ionic diffusivity and conductivity in the predicted materials are calculated using ab initio molecular dynamics (AIMD) based on DFT. The simulations are performed on the canonical ensemble with a time step of 2 fs, and the temperature was initialized at 100 K and elevated to the appropriate temperature (600, 720, 900, 1200, and 1500 K) with simulations lasting 200 ps for statistical analysis. Each supercell consists of four formula units (84 atoms). A γ-point-only sampling of k-space and a lower but sufficient plane-wave energy cutoff than for the structural optimization calculation was used (400, 280, and 270 eV for oxides, sulfides, and selenides, respectively). The Na diffusivity was calculated from atomic trajectories, and the activation energy and extrapolation to room-temperature diffusivity were obtained assuming Arrhenius behavior. Details of the simulation process can be found in previous work.[7,19,24]

Na-Ion Migration Barrier Calculations. Migration barriers for a Na^+ ion within perfect anion (O^{2-} or S^{2-}) bcc/fcc lattices were calculated using the nudged elastic band method[29] (NEB) in a large supercell comprising 3 × 3 × 3 conventional unit cells to minimize the interaction between the periodic images. A 2 × 2 × 2 k-point grid and kinetic energy cutoff of 520 eV were used for all NEB calculations. The supercells containing excess electrons were compensated for by a uniform background charge. The anion lattice was fixed, and only the migrating Na ion was allowed to relax.

Phase Stability Analysis. Thermodynamic stability was evaluated using calculated DFT total energies. The stability of any phase was evaluated by comparing its energy to linear combinations of the energy of other phases (leading to the same composition) using the convex hull construction. The stability analysis was performed vs all compounds present in the Inorganic Crystal Structure Database (ICSD)[30] plus our internal database of new compounds generated with data-mined substitution rules.[31] The stability was quantified by evaluating the energy above the hull, which represents the magnitude of a compound's decomposition energy. The value of the energy above the hull is non-negative and measures the thermodynamic driving force for the compound to decompose into a set of alternate phases.

Considering the significant overestimation of the binding energy of ground-state sulfur and selenium by the GGA-PBE functional, we have followed previous approaches[32,33] and applied constant energy corrections of −0.66 eV per S atom and −0.51 eV per Se atom in the phase stability analysis for sulfides and selenides, respectively. These correction energies, which correct for both the overbinding and the incomplete cancellation of self-interaction error in decomposition reactions which involve charge transfer between ions (such as oxidation of S^{2-} to S), were estimated by comparing the DFT and experimental formation energies for main group sulfides (same as ref 33) and selenides.[34]

The effect of phonons on the finite-temperature phase stability is calculated using the VASP implementation of density functional perturbation theory (DFPT) and the PHONOPY software package.[35] Thermodynamic quantities such as the Gibbs free energy and vibrational entropy were computed from the phonon spectrum. The phonon calculations were performed for all predicted new phases as well as their possible decomposition products in orthorhombic supercells with lattice vectors as close as possible to 20 Å.

DOI: 10.1021/acs.chemmater.7b02476
Chem. Mater. 2017, 29, 7475−7482

RESULTS AND DISCUSSION

Crystal Structure. In the reported experimental crystal structure of $Li_7P_3S_{11}$ or $Li_7(PS_4)(P_2S_7)$, both PS_4^{3-} thiophosphate and $P_2S_7^{4-}$ pyro-thiophosphate (two PS_4 tetrahedra share one corner S atom) groups are present, with Li atoms filling the substantially distorted tetrahedral cavities formed by the S anions.[36] This structure was adopted as the starting crystal structure for the optimization of $Li_7P_3X_{11}$ (X = O, Se) and $Na_7P_3X_{11}$ (X = O, S, Se) via chemical substitutions of Li with Na and S with O or Se. The optimized lattice parameters are listed in Table 1. The predicted structural parameters of these chemically substituted compounds obtained from DFT optimizations are very similar to that of $Li_7P_3S_{11}$ (triclinic centrosymmetric space group $P\bar{1}$). The unit-cell volumes of the lithium and sodium oxide compounds are 47−50% smaller than the corresponding sulfide compounds, while the selenium versions have 16−17% larger volumes than the corresponding sulfide compound. These differences are due to the anionic radii difference among O^{2-}, S^{2-}, and Se^{2-}, consistent with the findings in a previous study of the $Li_{10}GeP_2S_{12}$ family.[11] The volumes of sodium compounds are around 22−30% larger than the lithium counterparts, due to the larger ionic radii of Na^+ (115 pm) compared to Li^+ (90 pm).

Using a structure matching algorithm,[24] we confirmed that all calculated $Li_7P_3X_{11}$ (X = O, Se) and $Na_7P_3X_{11}$ (X = S, O and Se) structures have a bcc-like anion framework. The mapping of anion sublattice of $Na_7P_3S_{11}$ to a bcc lattice is given as an example shown in Figure 1.

Ionic Diffusivity and Conductivity. AIMD simulations were performed for all $Li_7P_3X_{11}$ and $Na_7P_3X_{11}$ (X = O, S, Se) materials. For the sulfides and selenides, diffusion calculations are performed at temperatures between 600 and 1200 K without melting of the crystal structure. For the oxides, calculations are performed at relatively higher temperatures (720−1500 K) due to the low ionic diffusivities obtained from poor trajectory samplings below 720 K. The calculated ionic diffusivities are shown in the Arrhenius plots in Figure 2. The activation energies obtained from the Arrhenius plots and the extrapolated room-temperature conductivities are summarized in Table. 2.

We find that the calculated ionic diffusivities in the $Na_7P_3X_{11}$ compounds are slightly lower than in the Li counterparts, and the corresponding activation energies for Na conductors are slightly larger. Nonetheless, the difference in alkali-ion conductivity between $Li_7P_3X_{11}$ and $Na_7P_3X_{11}$ compounds for a given type of anions is relatively small especially in the cases of sulfides and selenides; e.g., the activation energies for $Li_7P_3S_{11}$ and $Na_7P_3S_{11}$ are 0.191 and 0.217 eV, respectively. However, the calculated diffusivities are strongly dependent on the anion for both $Li_7P_3X_{11}$ and $Na_7P_3X_{11}$. The extrapolated RT conductivity increases by several orders of magnitude as one moves from an oxide to a sulfide or selenide, despite the structures all having very similar bcc-type anion lattice. For both Li and Na cases, little gain in diffusivity is achieved when going from sulfide to selenide. This behavior of diffusivity with anion substitution in $Li_7P_3X_{11}$ and $Na_7P_3X_{11}$ is also similar to the findings for $Li_{10}GeP_2X_{12}$ compounds as X changes from O to S and Se by Ong et al.[11]

Na Diffusion Pathway and Energy Landscape in $Na_7P_3X_{11}$. To better understand why the anion substitution has such an effect on the ionic conductivity of $Na_7P_3X_{11}$, we analyze the Na diffusion pathways by calculating the ionic probability densities obtained from AIMD simulations, and the Na energy landscape by calculating the Na site energies within the crystal structures. The results are shown in Figure 3, with the Na sites classified in the same way as the Li sites in the experimentally determined crystal structure of $Li_7P_3S_{11}$ from ref 36. The site energy at each site i is defined as the negative of the vacancy energy referenced to the average vacancy energy: $E^i_{site} = \sum_i E^i_{vacancy}/n - E^i_{vacancy}$, where $E^i_{vacancy}$ is the total energy of the

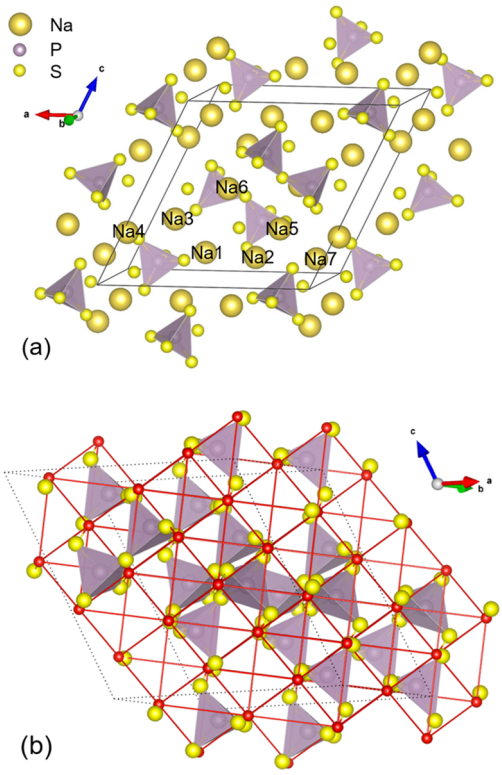

Figure 1. (a) Calculated crystal structure of $Na_7P_3S_{11}$ and (b) mapping of the sulfur sublattice to a bcc framework in $Na_7P_3S_{11}$ using the structural matching algorithm. S atom, PS_4 tetrahedra, and the matching bcc lattice are colored yellow, purple, and red, respectively. The Na sites in panel a are numbered in the same way as the Li sites in $Li_7P_3S_{11}$ in ref 36. The mapped structure in panel b is plotted under a different angle without showing the Na atoms for a better view of the bcc anion arrangement.

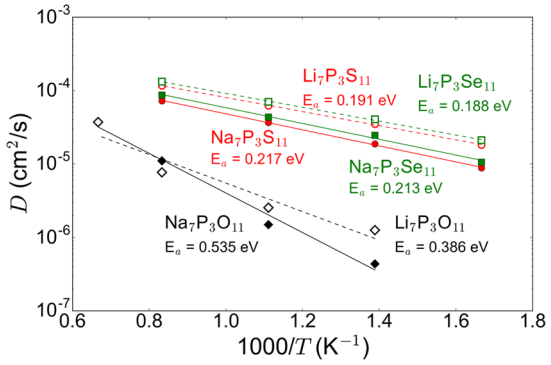

Figure 2. Arrhenius plots of calculated Li and Na diffusivities in $Li_7P_3X_{11}$ and $Na_7P_3X_{11}$ (X = O, S, Se). The lines are least-squares fits to the diffusivity data at 600, 720, 900, and 1200 K for sulfides and selenides. For oxides the simulations are performed at 720, 900, 1200, and 1500 K.

DOI: 10.1021/acs.chemmater.7b02476
Chem. Mater. 2017, 29, 7475−7482

Table 2. Calculated Activation Energy and Extrapolated RT Conductivity for Ionic Conductors $Li_7P_3X_{11}$ and $Na_7P_3X_{11}$ (X = O, S, and Se)

composition	activation energy (eV)	RT conductivity (mS/cm)
$Li_7P_3O_{11}$	0.386	0.03
$Li_7P_3S_{11}$	0.191	45.66
$Li_7P_3Se_{11}$	0.188	47.94
$Na_7P_3O_{11}$	0.535	0.003
$Na_7P_3S_{11}$	0.217	10.97
$Na_7P_3Se_{11}$	0.213	12.56

unit cell containing a Na vacancy at the site, and n is the total number of Na sites in the structure.

The probability density analysis on the distribution of Na ions demonstrates that the ionic conduction in $Na_7P_3S_{11}$ and $Na_7P_3Se_{11}$ occurs through a three-dimensional diffusion network connecting all seven distinct crystallographic sites (Figure 3, left panels), very similar to the case of $Li_7P_3S_{11}$ (see refs 18 and 24). The evenly distributed probability densities indicate that Na ions have a relatively flat energy landscape along the channels, which can also be seen from the calculated Na site energies (Figure 3, right panels) in $Na_7P_3S_{11}$ and $Na_7P_3Se_{11}$. Our Na site energies of $Na_7P_3S_{11}$ are in good agreement with the calculated Li vacancy energies of $Li_7P_3S_{11}$ at the corresponding sites by Holzwarth et al.[37]

In contrast, the Na probability densities in $Na_7P_3O_{11}$ are mostly isolated as shown in Figure 3. Na diffusion is mainly through the adjacent Na2 and Na3 sites in $Na_7P_3O_{11}$, as the two sites are very close in energy. The site energy difference between adjacent Na sites for ionic migration is usually a lower bound for the activation energy, as additional energy is often required to migrate between two sites, even if they have similar energy.[24] In the case of $Na_7P_3O_{11}$, the site energy changes along the diffusion path connected by adjacent Na site pairs (e.g., Na1−Na2, Na3−Na4, and Na4−Na7) are much larger than $Na_7P_3S_{11}$ and $Na_7P_3Se_{11}$. This indicates a greater activation energy in $Na_7P_3O_{11}$ than in the other compounds, which agrees well with the results from the AIMD simulations.

For all three cases, the two Na sites between two $P_2X_7^{4-}$ ditetrahedra units, Na5 and Na6, have higher energy than the other sites surrounding the single PX_4^{3-} tetrahedron (Na1, Na2, Na3, Na4, and Na7). The higher site energies at Na5 and Na6 are likely due to stronger Columbic repulsion from the adjacent P^{5+} cations in the $P_2X_7^{4-}$ ditetrahedra units. Although the anion frameworks are almost identical in the three cases, oxygen is less polarizable than sulfur and selenium and the distance between Na^+ and P^{5+} are much shorter in $Na_7P_3O_{11}$ than in the sulfide and selenide structures. Therefore, stronger interactions between the cations result in greater Na site energy variations in the $Na_7P_3O_{11}$ energy landscape.

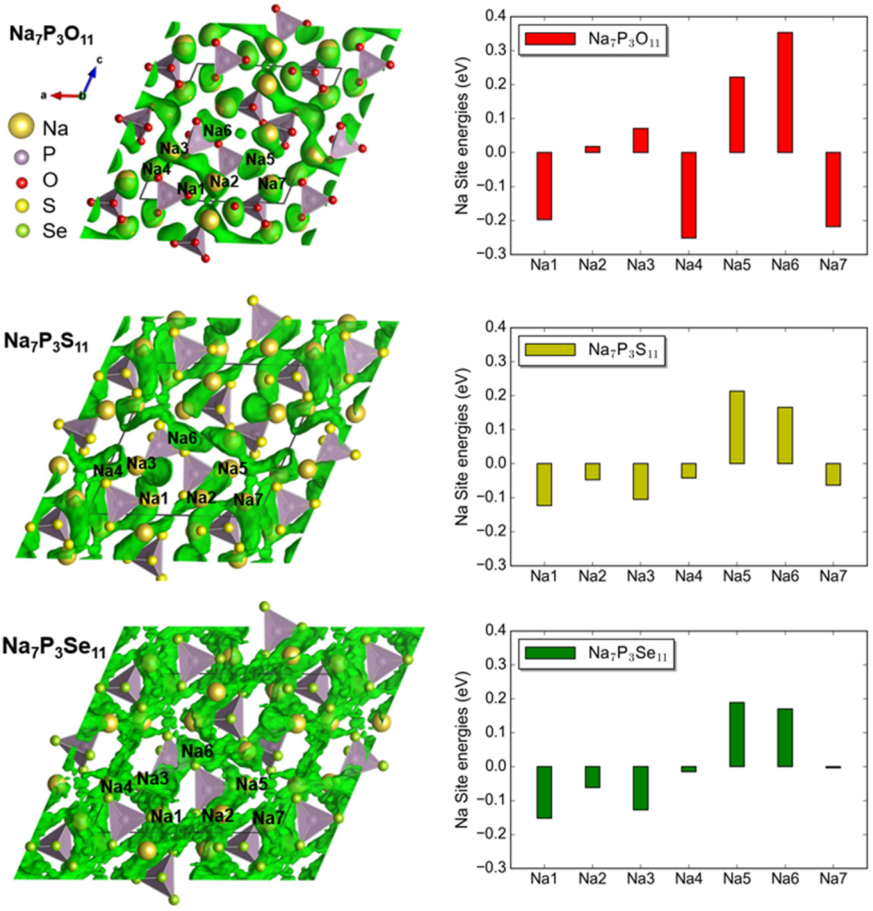

Figure 3. Calculated Na-ion probability densities (left) and Na site energies (right) in $Na_7P_3X_{11}$ (X = O, S, and Se). The probability densities of Na ions are obtained from ab initio molecular dynamics simulations at 900 K with 200 ps, and the isosurfaces are plotted at isovalues of $2P_0$ where P_0 is defined as the mean value of the density. The Na site energy at each site is defined as the negative energy of a Na-ion vacancy referenced to the average of all site energies (see text for the formulation).

DOI: 10.1021/acs.chemmater.7b02476
Chem. Mater. 2017, 29, 7475−7482

Table 3. Predicted 0 K Phase Stability and Phase Equilibria for Ionic Conductors $Li_7P_3X_{11}$ and $Na_7P_3X_{11}$ (X = O, S, and Se)[a]

composition	stability at 0 K (energy above hull) meV/atom	meV/f.u.	decomposition products
$Li_7P_3O_{11}$	25.5	537	Li_3PO_4, $Li_4P_2O_7$
$Li_7P_3S_{11}$	12.4 (28.3)	260 (594)	Li_3PS_4, P_2S_5 (Li_3PS_4, $Li_4P_2S_6$, S)
$Li_7P_3Se_{11}$	11.1 (38.2)	233 (802)	Li_3PSe_4*, P_2Se_5 ($Li_4P_2Se_6$, Li_2Se, Se)
$Na_7P_3O_{11}$	14.5	304	Na_3PO_4, $Na_4P_2O_7$
$Na_7P_3S_{11}$	10.5 (23.2)	221 (487)	Na_3PS_4, $Na_4P_2S_7$* (Na_3PS_4, $Na_4P_2S_6$, S)
$Na_7P_3Se_{11}$	11.9 (25.0)	250 (525)	Na_3PSe_4, $NaPSe_3$* ($Na_4P_2Se_6$, Na_3PSe_4, Se)

[a]The phase stability and equilibria results without sulfur/selenium energy corrections are listed in parentheses. The decomposed products marked with an asterisk (*) are predicted stable phases derived from existing compounds in ICSD (Li_3PSe_4 derived from ICSD-Li_3PS_4; $Na_4P_2S_7$ derived from ICSD-$Li_4P_2S_7$; $NaPSe_3$ derived from ICSD-$KPSe_3$).

Phase Stability. In Table 3 we show the 0 K phase equilibria and decomposition energies calculated from the Li(Na)−P−X (X = O, S, and Se) ternary phase diagrams constructed from DFT formation energies. It is known that the experimentally discovered $Li_7P_3S_{11}$ is a high-temperature crystalline phase which can be precipitated from the Li_2S−P_2S_5 glasses.[36,38] Consistent with previous computational studies,[17,18,37] $Li_7P_3S_{11}$ is calculated to be a metastable phase at low temperature with a driving force to decompose to lower energy compounds such as Li_3PS_4 and $Li_4P_2S_6$.

Similar to $Li_7P_3S_{11}$, we find the calculated $Li_7P_3X_{11}$ (X = O, and Se) and $Na_7P_3X_{11}$ (X = O, S, and e) all to be metastable at 0 K. In general, the oxides are predicted to have a relatively higher driving force for decomposition than the corresponding sulfides and selenides, due to the high intrinsic stability of the competing decomposition products A_3PO_4 and $A_4P_2O_7$ (A = Li or Na). For the sulfides and selenides, the predicted phase equilibria depend on the S/Se chemical potential, i.e., whether we apply sulfur/selenium energy corrections to the DFT energies (see Methods). Nonetheless, the sulfides are likely to decompose to more stable ternary sulfides such as Li_3PS_4 or Na_3PS_4, and the selenide breakdown would consist of more stable Li_3PSe_4 or Na_3PSe_4 with other ternaries or binaries to balance the composition.

To evaluate the stability of $Li_7P_3X_{11}$ and $Na_7P_3X_{11}$ at finite temperature, we also consider the vibrational entropy contributions to the thermodynamic stability. Figure 4 shows the calculated temperature-dependent Gibbs free energy of $Li_7P_3X_{11}$ and $Na_7P_3X_{11}$ referenced to the predicted decomposition products from Table 3. The effect of phonon stabilization is found to be more profound in the case of $Li_7P_3S_{11}$ than for the other compounds. At a temperature above 730 K the phonon contribution of over 0.26 eV/f.u. to the total free energy is able to stabilize the phase of $Li_7P_3S_{11}$ against decomposition, and this transition temperature is close to the findings by Ong et al. (630 K from computations and 553 K from experiments).[18] However, the calculated phonon free energies indicate that none of the other compounds could be thermodynamically stable even at 1000K. The phonon free energies in the Na compounds are especially small, likely due to comparable phonon contribution in the decomposed Na_3PX_4 (X = O, S, and Se) with their highly mobile Na sublattice.[7,39]

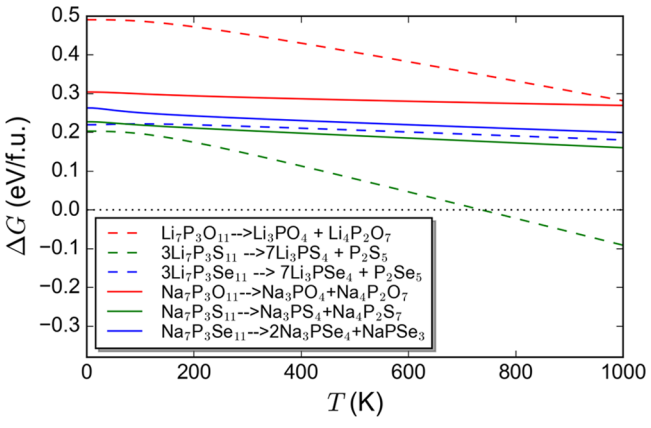

Figure 4. Calculated temperature-dependent Gibbs free energy change of the reverse decomposition reaction for $Li_7P_3X_{11}$ and $Na_7P_3X_{11}$ (X = O, S, and Se). The black dashed line indicates zero ΔG.

DISCUSSION

Ionic Conductivity of bcc-Type Oxide vs Sulfide. The predicted Na-ion conductors are additions to the growing family of alkali ionic conductors with a bcc anion framework and exceptionally high ionic conductivity.[10,24,40] The RT conductivities predicted, 10.97 mS cm^{-1} for $Na_7P_3S_{11}$ and 12.56 mS cm^{-1} for $Na_7P_3Se_{11}$, are significantly higher than that of any known solid Na-ion sulfide or selenide conductor. The predicted ionic conductivity in $Na_7P_3O_{11}$ is, however, much lower than the other two compounds with similar structures, consistent with a previous study[11] that oxygen substituted $Li_{10}GeP_2O_{12}$ has much lower conductivity as compared to $Li_{10}GeP_2S_{12}$.

Based on the bcc anion backbone alone, the predicted low ionic conductivity seen in $Na_7P_3O_{11}$ simulations is an anomaly. High ionic conductivity requires a flat energy landscape with sites at equivalent energy along the migration pathway, and a bcc anion lattice can provide such low activation energy crystallographic backbone.[24] The bcc descriptor explains very well the superionic behavior in Li sulfide ionic conductors such as $Li_{10}XP_2S_{12}$ (X = Ge, Sn, and Si) and $Li_7P_3S_{11}$. Sodium ions behave similarly in both ideal bcc (fcc) O^{2-} and S^{2-} lattices, as shown in Figure 5, where the calculated energy barrier for the Na migration in a bare bcc anion lattice (Figure 5a) is significantly lower than that in a fcc anion lattice (Figure 5b). Comparison between the AIMD activation energies for $Na_7P_3S_{11}$ and $Na_{10}XP_2S_{12}$(M = Si, Ge, and Sn)[10] with the Na migration barriers estimated from the bare bcc S^{2-} host indicates that these conductors are close to ideal at a given volume. In contrast with the sulfides, however, we find a large difference between the AIMD calculated activation energy of $Na_7P_3O_{11}$ (0.54 eV) and the activation barrier for Na ion migration in the empty bcc O^{2-} lattice (0.30 eV) at the same volume, indicating that the arrangement of the P^{5+} cations in $Na_7P_3O_{11}$ perturbs the Na energy landscape in an unfavorable

DOI: 10.1021/acs.chemmater.7b02476
Chem. Mater. 2017, 29, 7475−7482

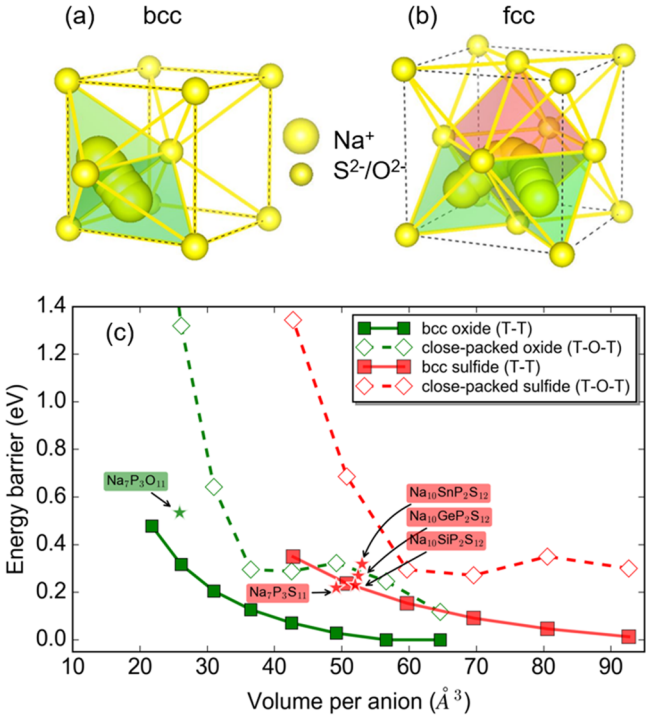

Figure 5. (a) Na-ion migration pathway in a bcc anion lattice. (b) Na-ion migration pathway in a fcc anion lattice. (c) Activation barrier calculated for the Na-ion migration pathways in the bcc and close-packed (fcc) O^{2-} and S^{2-} lattices at different volumes. The volume ranges are selected according to the Na containing oxides and sulfides in the Inorganic Crystal Structure Database (ICSD).[30] T−T and T−O−T refer to the two pathways connecting tetrahedral sites in bcc and fcc lattices, respectively.[24] Solid and dotted lines are guides to the eye. Activation energies calculated for bcc-type conductors $Na_7P_3X_{11}$ (X = O or S) in this work and $Na_{10}MP_2S_{12}$ (M = Si, Ge, or Sn) from ref 10 are marked by star symbols for comparison.

way. The interactions between the Na and non-Na cations, P^{5+}, though small in sulfides and selenides, play a large role in the relatively smaller anion lattice of O^{2-} in $Na_7P_3O_{11}$, nearly doubling the activation energy from that of the bare O^{2-} lattice. As the positions of these non-Na cations are often not evenly distributed in the lattice, such effects inevitably result in a corrugated Na energy landscape. This is demonstrated by the comparison of calculated site energies in $Na_7P_3O_{11}$ and $Na_7P_3S_{11}$ where we clearly find the Na energy landscape is much more affected by the arrangement of P^{5+} cations in the oxide than that of the sulfide.

Although we predict higher ionic conductivities in the sulfide and selenides, it is expected that the oxides would have better electrochemical stability than the sulfides and selenides. Such a trend has been confirmed in previous theoretical and experimental studies in similar compositions such as Li_3PO_4/Li_3PS_4 (see ref 12) and Na_3PS_4/Na_3PSe_4 (see ref 41). The interfacial stability of the predicted $Na_7P_3X_{11}$ (X = O, S, and Se) conductors and their compatibility against various battery electrodes are worth further investigation.

Synthesizability of the Predicted Na Ionic Conductors. Although the predicted Na ionic conductors $Na_7P_3X_{11}$ (X = O or S) have similar phase stability as $Li_7P_3S_{11}$ with comparable driving force for decomposition at 0 K, our thermodynamic analysis from phase diagrams and phonon free energy calculations indicates that these sodium compounds may not be thermodynamically stable even at elevated temperatures as high as 1000 K. Unlike $Li_7P_3S_{11}$ which is found to have a relatively large vibrational entropy and can therefore be stable at an elevated temperature, the sodium counterparts all suffer from relatively lower entropic free energy contribution as compared to the predicted decomposition products such as Na_3PX_4 (X = O or S). This indicates that it may be more difficult to synthesize the predicted Na compounds by the same thermal-treatment method used for the synthesis of $Li_7P_3S_{11}$. Our theoretical analysis of the possible competing phases for $Na_7P_3S_{11}$ matches very well with the findings from a recent experimental study by Houtarde et al., which attempted to synthesize $Na_7P_3S_{11}$ by heat-treatment and quenching of 70−30 Na_2S−P_2S_5 with high temperature up to 773 K, and only Na_3PS_4 and $Na_4P_2S_7$ were found after the synthesis.[42]

It may be possible to improve the phase stability and the chance of synthesizability of the predicted Na_3PX_4 (X = O or S) compounds by adding site disorder through doping of the anion sites therefore increase the entropic contributions. Similar to the recently discovered oxysulfides in the $Li_{10}GeP_2S_{12}$ family,[43] solid solutions may be formed among the $Na_7P_3O_{11}$, $Na_7P_3S_{11}$ and $Na_7P_3Se_{11}$ as the three compounds have very similar crystalline structures, providing an avenue to fine-tune phase stability and ionic conductivity. Li/Na ion exchange could be another possible method to obtain $Na_7P_3S_{11}$ from the Li phase $Li_7P_3S_{11}$, which has been successfully applied to synthesize novel cathode materials.[44−46] The DFT calculated enthalpy of formation for the solid-state reaction of $Li_7P_3S_{11}$ + NaF → $Na_7P_3S_{11}$ + LiF is −2.05 eV (−197 kJ mol^{-1}) which indicates the possibility of such ion exchange reaction.

CONCLUSIONS

By using first-principles calculations, we have evaluated the possible derivatives of the known lithium ionic conductor $Li_7P_3S_{11}$ and predicted a class of new sodium ionic conductors $Na_7P_3X_{11}$ (X = O, S, and Se). The predicted Na-containing compounds have extraordinarily high ionic conductivity at RT, exceeding the performance of currently known Na-ion solid-state conductors. We hope this study stimulates further experimental exploration in the predicted chemistry for better ionic conductors.

AUTHOR INFORMATION

Corresponding Authors

*(Y.W.) E-mail: eric.wangyan@samsung.com.
*(G.C.) E-mail: gceder@berkeley.edu.

ORCID

Yan Wang: 0000-0002-8648-2172

Present Address

#(S.-H.B.) University of Michigan-Shanghai Jiao Tong University Joint Institute, Shanghai Jiao Tong University, Shanghai 200240, P. R. China.

Notes

The authors declare no competing financial interest.

ACKNOWLEDGMENTS

This work was supported by Samsung Advanced Institute of Technology, and computational resources were provided by the Extreme Science and Engineering Discovery Environment (XSEDE), which is supported by the National Science Foundation Grant No. ACI-1548562.

DOI: 10.1021/acs.chemmater.7b02476
Chem. Mater. 2017, 29, 7475−7482

REFERENCES

(1) Motavalli, J. Technology: A solid future. *Nature* **2015**, *526*, S96−S97.

(2) Kamaya, N.; Homma, K.; Yamakawa, Y.; Hirayama, M.; Kanno, R.; Yonemura, M.; Kamiyama, T.; Kato, Y.; Hama, S.; Kawamoto, K.; Mitsui, A. A lithium superionic conductor. *Nat. Mater.* **2011**, *10*, 682−6.

(3) Seino, Y.; Ota, T.; Takada, K.; Hayashi, A.; Tatsumisago, M. A sulphide lithium super ion conductor is superior to liquid ion conductors for use in rechargeable batteries. *Energy Environ. Sci.* **2014**, *7*, 627−631.

(4) Kummer, J. T. *β*-Alumina electrolytes. *Prog. Solid State Chem.* **1972**, *7*, 141−175.

(5) Goodenough, J. B.; Hong, H. Y.-P.; Kafalas, J. A. Fast Na+-ion transport in skeleton structures. *Mater. Res. Bull.* **1976**, *11*, 203−220.

(6) Hayashi, A.; Noi, K.; Sakuda, A.; Tatsumisago, M. Superionic glass-ceramic electrolytes for room-temperature rechargeable sodium batteries. *Nat. Commun.* **2012**, *3*, 856.

(7) Bo, S. H.; Wang, Y.; Kim, J. C.; Richards, W. D.; Ceder, G. Computational and Experimental Investigations of Na-Ion Conduction in Cubic Na3PSe4. *Chem. Mater.* **2016**, *28*, 252−258.

(8) Zhang, L.; Yang, K.; Mi, J.; Lu, L.; Zhao, L.; Wang, L.; Li, Y.; Zeng, H. Na3PSe4: A Novel Chalcogenide Solid Electrolyte with High Ionic Conductivity. *Adv. Energy Mater.* **2015**, *5*, 1501294.

(9) Wang, H.; Chen, Y.; Hood, Z. D.; Sahu, G.; Pandian, A. S.; Keum, J. K.; An, K.; Liang, C. An Air-Stable Na3SbS4 Superionic Conductor Prepared by a Rapid and Economic Synthetic Procedure. *Angew. Chem., Int. Ed.* **2016**, *55*, 8551−8555.

(10) Richards, W. D.; Tsujimura, T.; Miara, L. J.; Wang, Y.; Kim, J. C.; Ong, S. P.; Uechi, I.; Suzuki, N.; Ceder, G. Design and synthesis of the superionic conductor Na10SnP2S12. *Nat. Commun.* **2016**, *7*, 11009.

(11) Ong, S. P.; Mo, Y.; Richards, W. D.; Miara, L.; Lee, H. S.; Ceder, G. Phase stability, electrochemical stability and ionic conductivity of the $Li_{10\pm1}MP_2X_{12}$ (M = Ge, Si, Sn, Al or P, and X = O, S or Se) family of superionic conductors. *Energy Environ. Sci.* **2013**, *6*, 148−156.

(12) Richards, W. D.; Miara, L. J.; Wang, Y.; Kim, J. C.; Ceder, G. Interface Stability in Solid-State Batteries. *Chem. Mater.* **2016**, *28*, 266−273.

(13) Zhu, Y.; He, X.; Mo, Y. First principles study on electrochemical and chemical stability of solid electrolyte−electrode interfaces in all-solid-state Li-ion batteries. *J. Mater. Chem. A* **2016**, *4*, 3253−3266.

(14) Chen, H. M.; Maohua, C.; Adams, S. Stability and ionic mobility in argyrodite-related lithium-ion solid electrolytes. *Phys. Chem. Chem. Phys.* **2015**, *17*, 16494−16506.

(15) Radhakrishnan, B.; Ong, S. P. Aqueous Stability of Alkali Superionic Conductors from First-Principles Calculations. *Front. Energy Res.* **2016**, *4*, 1−12.

(16) Deng, Z.; Wang, Z.; Chu, I.-H.; Luo, J.; Ong, S. P. Elastic Properties of Alkali Superionic Conductor Electrolytes from First Principles Calculations. *J. Electrochem. Soc.* **2016**, *163*, A67−A74.

(17) Holzwarth, N. a. W.; Lepley, N. D.; Du, Y. a. Computer modeling of lithium phosphate and thiophosphate electrolyte materials. *J. Power Sources* **2011**, *196*, 6870−6876.

(18) Chu, I.; Nguyen, H.; Hy, S.; Lin, Y.; Wang, Z.; Xu, Z.; Deng, Z.; Meng, Y. S.; Ong, S. P. Insights into the Performance Limits of the $Li_7P_3S_{11}$ Superionic Conductor: A Combined First-Principles and Experimental Study. *ACS Appl. Mater. Interfaces* **2016**, *8*, 7843−7853.

(19) Mo, Y.; Ong, S. P.; Ceder, G. First Principles Study of the $Li_{10}GeP_2S_{12}$ Lithium Super Ionic Conductor Material. *Chem. Mater.* **2012**, *24*, 15−17.

(20) Yu, C.; Ganapathy, S.; de Klerk, N. J. J.; Roslon, I.; van Eck, E. R. H.; Kentgens, A. P. M.; Wagemaker, M. Unravelling Li-Ion Transport from Picoseconds to Seconds: Bulk versus Interfaces in an Argyrodite Li_6PS_5Cl−Li_2S All-Solid-State Li-Ion Battery. *J. Am. Chem. Soc.* **2016**, *138*, 11192−11201.

(21) Bron, P.; Johansson, S.; Zick, K.; Schmedt auf der Gunne, J.; Dehnen, S.; Roling, B. $Li_{10}SnP_2S_{12}$: An Affordable Lithium Superionic Conductor. *J. Am. Chem. Soc.* **2013**, *135*, 15694−15697.

(22) Kuhn, A.; Gerbig, O.; Zhu, C.; Falkenberg, F.; Maier, J.; Lotsch, B. V. A new ultrafast superionic Li-conductor: ion dynamics in $Li_{11}Si_2PS_{12}$ and comparison with other tetragonal LGPS-type electrolytes. *Phys. Chem. Chem. Phys.* **2014**, *16*, 14669−74.

(23) Whiteley, J. M.; Woo, J. H.; Hu, E.; Nam, K.-W.; Lee, S.-H. Empowering the Lithium Metal Battery through a Silicon-Based Superionic Conductor. *J. Electrochem. Soc.* **2014**, *161*, A1812−A1817.

(24) Wang, Y.; Richards, W. D.; Ong, S. P.; Miara, L. J.; Kim, J. C.; Mo, Y.; Ceder, G. Design principles for solid-state lithium superionic conductors. *Nat. Mater.* **2015**, *14*, 1026−1031.

(25) Kresse, G.; Furthmuller, J. Efficient iterative schemes for ab initio total-energy calculations using a plane-wave basis set. *Phys. Rev. B: Condens. Matter Mater. Phys.* **1996**, *54*, 11169−11186.

(26) Perdew, J. P.; Burke, K.; Ernzerhof, M. Generalized Gradient Approximation Made Simple. *Phys. Rev. Lett.* **1996**, *77*, 3865−3868.

(27) Ong, S. P.; Richards, W. D.; Jain, A.; Hautier, G.; Kocher, M.; Cholia, S.; Gunter, D.; Chevrier, V. L.; Persson, K. a.; Ceder, G. Python Materials Genomics (pymatgen): A robust, open-source python library for materials analysis. *Comput. Mater. Sci.* **2013**, *68*, 314−319.

(28) Momma, K.; Izumi, F. VESTA 3 for three-dimensional visualization of crystal, volumetric and morphology data. *J. Appl. Crystallogr.* **2011**, *44*, 1272−1276.

(29) Henkelman, G.; Uberuaga, B. P.; Jónsson, H. A climbing image nudged elastic band method for finding saddle points and minimum energy paths. *J. Chem. Phys.* **2000**, *113*, 9901−9904.

(30) *Inorganic Crystal Structure Database*; http://icsd.fiz-karlsruhe.de/icsd/.

(31) Hautier, G.; Fischer, C.; Ehrlacher, V.; Jain, A.; Ceder, G. Data mined ionic substitutions for the discovery of new compounds. *Inorg. Chem.* **2011**, *50*, 656−663.

(32) Wang, L.; Maxisch, T.; Ceder, G. Oxidation energies of transition metal oxides within the GGA + U framework. *Phys. Rev. B: Condens. Matter Mater. Phys.* **2006**, *73*, 195107.

(33) Zhu, Z.; Chu, I.-H.; Deng, Z.; Ong, S. P. Role of Na + Interstitials and Dopants in Enhancing the Na + Conductivity of the Cubic Na_3PS_4 Superionic Conductor. *Chem. Mater.* **2015**, *27*, 8318−8325.

(34) Olin, Å.; Noläng, B.; Öhman, L.-O.; Osadchii, E.; Rosén, E. *Chemical thermodynamics of selenium*, Vol. 7; Elsevier Science: Amsterdam, 2005.

(35) Togo, A.; Tanaka, I. First principles phonon calculations in materials science. *Scr. Mater.* **2015**, *108*, 1−5.

(36) Yamane, H.; Shibata, M.; Shimane, Y.; Junke, T.; Seino, Y.; Adams, S.; Minami, K.; Hayashi, A.; Tatsumisago, M. Crystal structure of a superionic conductor, Li7P3S11. *Solid State Ionics* **2007**, *178*, 1163−1167.

(37) Lepley, N. D.; Holzwarth, N. a. W. Computer Modeling of Crystalline Electrolytes: Lithium Thiophosphates and Phosphates. *J. Electrochem. Soc.* **2012**, *159*, A538−A547.

(38) Mizuno, F.; Hayashi, A.; Tadanaga, K.; Tatsumisago, M. High lithium ion conducting glass-ceramics in the system Li2S−P2S5. *Solid State Ionics* **2006**, *177*, 2721−2725.

(39) Bo, S.-H.; Wang, Y.; Ceder, G. Structural and Na-ion conduction characteristics of Na 3 PS x Se 4−x. *J. Mater. Chem. A* **2016**, *4*, 9044−9053.

(40) Richards, W. D.; Wang, Y.; Miara, L. J.; Kim, J. C.; Ceder, G. Design of $Li_{1+2x}Zn_{1-x}PS_4$, a new lithium ion conductor. *Energy Environ. Sci.* **2016**, *9*, 3272−3278.

(41) Tian, Y.; Shi, T.; Richards, W. D.; Li, J.; Kim, J. C.; Bo, S.; Ceder, G. Compatibility issues between electrodes and electrolytes in solid-state batteries. *Energy Environ. Sci.* **2017**, *10*, 1150−1166.

(42) Houtarde, D. Synthesis of Sulfide-based Solid Electrolytes for Application to All-Solid-State Lithium-Sulfur Batteries. Master's Thesis; University of Waterloo, Waterloo, Ontario, 2015.

(43) Suzuki, K.; Sakuma, M.; Hori, S.; Nakazawa, T.; Nagao, M.; Yonemura, M.; Hirayama, M.; Kanno, R. Synthesis, structure, and electrochemical properties of crystalline Li-P-S-O solid electrolytes:

DOI: 10.1021/acs.chemmater.7b02476
Chem. Mater. 2017, 29, 7475−7482

Novel lithium-conducting oxysulfides of $Li_{10}GeP_2S_{12}$ family. *Solid State Ionics* **2016**, *288*, 229−234.
(44) Armstrong, a. R.; Bruce, P. G. Synthesis of layered LiMnO2 as an electrode for rechargeable lithium batteries. *Nature* **1996**, *381*, 499−500.
(45) Gaubicher, J.; Wurm, C.; Goward, G.; Masquelier, C.; Nazar, L. Rhombohedral Form of Li 3 V 2 (PO 4) 3 as a Cathode in Li-Ion Batteries. *Chem. Mater.* **2000**, *12*, 3240−3242.
(46) Chen, H.; Hautier, G.; Jain, A.; Moore, C.; Kang, B.; Doe, R.; Wu, L.; Zhu, Y.; Tang, Y.; Ceder, G. Carbonophosphates: A New Family of Cathode Materials for Li-Ion Batteries Identified Computationally. *Chem. Mater.* **2012**, *24*, 2009−2016.

DOI: 10.1021/acs.chemmater.7b02476
Chem. Mater. 2017, 29, 7475−7482